EUROPEAN COMMISSION
DG RESEARCH

7th FRAMEWORK PROGRAMME

Collaborative Project - Small or medium-scale focused research project

Grant agreement no.: 218508

D9.2a

Exterior Acoustics Application Case: SEA of Sound Reduction Index of a Generic Trim Panel

Deliverable no.	D9.2a
Dissemination level (C/P)	P (Public)
Work Package	WP9
Author(s)	Mathias Barbagallo, Svante Finnveden, Jamil Renno
Co-author(s)	Neil Ferguson
Status (F: final, D: draft)	F
File Name	MID-MOD_D9_2a.pdf
Project Start Date and Duration	January 1 , 2009 – December 31 , 2011; 36 months

TABLE OF CONTENTS

1 Executive summary 4

2 The generic trim panel 4

2.1 SRI measurement 12

3 Statistical energy analysis employing an equivalent fluid 13

3.1 The equivalent fluid 17

4 Results 18

5 Acknowledgments 20

6 References 20

TABLES

Table 1 Specific porous materials data. † indicates educated guesses [2], whereas its absence direct measurements. 5

Table 2 General porous material data. 5

Table 3 Porous material parameters. 6

Table 4 Bulk modulus of the equivalent fluid [Pa]. 6

Table 5 Viscous drag [Pa.s/m^2] 7

Table 6 Young's modulus [Pa] and shear modulus [Pa] for *Grey*. 9

Table 7 Young's modulus [Pa] and shear modulus [Pa] for *Yellow*. 10

Table 8 Rubber mat's data. † indicates a guess. 10

Table 9 Rubber mats shear modulus [Pa]. 11

Table 10 Sound reduction index measurement in third-octave bands. 15

FIGURES

Figure 1 From left to right, the aluminium panel, *Grey* porous material and the rubber mat. The porous material is 2.24 cm thick. 4

Figure 2 Pins clamping the aluminium panel; the aluminium panel is in the lower half, the wooden frame is in between the two dashed lines and the top half is the rigid wall. The tape seals the gap between the wooden frame and the rigid wall. 8

Figure 3 Location of the metal pins on the aluminium panel. Distance **a**: 40.6 cm; Distance **b**: 9.6 cm; Distance **c**: 31.3 cm; Distance **d**: 39 cm. 8

Figure 4 White mastic sealing the gap between the rubber mat and the wooden frame. 12

Figure 5 Schematic sketch of the measurement set-up. 14

Figure 6 View of the multilayered structure from the reverberation room, where a rotating micrhophone measures the spatial-averaged rms pressure. 14

Figure 7 View of the multilayered structure from the anechoic room, where an intensity probe measures the time-averaged intensity. 16

Figure 8 Proposed SEA for a multilayered structure. **A**, mass impeded equivalent fluid-wall element ↔room channel; **B**, oblique equivalent fluid - wall element ↔room channel; **C**, rooms ↔room channel (mass law, non-resonant); **D**, room ↔wall channel; **E**, mass impeded plane equivalent fluid - wall element ↔wall channel; **F**, oblique equivalent fluid-wall element ↔channel; **G**, wall ↔wall channel (flanking transmission). 16

Figure 9 SRI for the multilayered structure comprising the *Grey* material: measurement (red curve with circles), SEA (blue dashed curve) and mass-law prediction (black dotted curve). The SEA model employs no direct coupling between the walls. 18

Figure 10 SRI for the multilayered structure comprising the *Yellow* material: measurement (red curve with circles), SEA (blue dashed curve) and mass-law prediction (black dotted curve). The SEA model employs no direct coupling between the walls. 19

Figure 11 SRI for the multilayered structure comprising the *Grey* material: measurement (red curve with circles), SEA (blue dashed curve) and mass-law prediction (black dotted curve). The SEA model employs a coupling loss factor of 2.5×10^{-3} between the walls. 19

Figure 12 SRI for the multilayered structure comprising the *Yellow* material: measurement (red curve with circles), SEA (blue dashed curve) and mass-law prediction (black dotted curve). The SEA model employs a coupling loss factor of 1.3×10^{-4} between the walls.....20

1 Executive summary

This report presents measurements of the sound reduction index (SRI) of two generic trim panels, together with a statistical energy analysis (SEA). The panels are multi-layered structures composed of an aluminium shell with single curvature to which a composite consisting of a rubber mat and a porous material is attached; two different composites are investigated. The SRI measurements have been performed at The Marcus Wallenberg Laboratory for Sound and Vibration Research (MWL) at the Royal Institute of Technology (KTH) in Stockholm.

The SRI of these panels is predicted by an SEA model, employing an equivalent fluid to model the porous material. The SEA may provide a deeper understanding of the physics of the investigated structures. Section 2 presents the structure under study and the sound reduction index measurement; Section 3 introduces the SEA of this kind of structure; Section 4 shows the SRI measurements and the SEA predictions.

2 The generic trim panel

The specimen is composed of a curved aluminium panel to which a composite is attached; the composite structure comprises porous foam and a rubber mat; two different kinds of composites are investigated: a composite Yellow and a composite Grey. The composite is glued to the aluminium panel. Figure 1 shows Grey attached to the aluminium panel.

Figure 1 From left to right, the aluminium panel, *Grey* porous material and the rubber mat. The porous material is 2.24 cm thick.

The aluminium panel and the composite have the same length and height of 900 mm x 920 mm. The panel has a radius of curvature of 3 m and a thickness of 1.5 mm. The quantities needed in Biot's model or in an equivalent fluid model are reported in Tables 1 and 5; see also Subsection 3.1 for more details on the latter. The elastic parameters of the porous materials are obtained via a fractional Kelvin-Voigt model for one of the Young's modulus and for one of the shear modulus of the porous material,

$$E_y(f) = E_0 \frac{1+(if/f_1)^\alpha}{1+(if/f_2)^\alpha}; \quad G_{xy}(f) = G_0 \frac{1+(if/f_1)^\beta}{1+(if/f_2)^\beta}, \tag{1}$$

where *f* is the frequency of vibration and the subscript *y* indicates the transverse direction of the composite; note that the estimation of these material parameters is based upon the assumption that:

$$E_x = E_y; \quad E_{xy} = 0.3E_y. \tag{2}$$

Tables 6 and 7 report the third-octave bands value for E_y and G_{xy}. The parameters G_0, ω_0 and α in Table 8 are employed in another fractional Kelvin-Voigt model for the rubber shear modulus,

$$\hat{G}(\omega) = G_0\left(1+\left(-\frac{i\omega}{\omega_0}\right)^\alpha\right), \tag{3}$$

which fits laboratory measurements. Table 9 reports the third-octave bands value for G: its real part provides the shear modulus, while the ratio of the imaginary and real parts the damping loss factors.

Table 1 Specific porous materials data. † indicates educated guesses [2], whereas its absence direct measurements.

Symbol	Quantity	*Grey*	*Yellow*
ρ_s	Porous material density $[kg/m^3]$	57.2	47.7
ϕ	Porosity $[-]$ †	0.95	0.957
d	Thickness $[m]$	2.24×10^{-2}	2.12×10^{-2}
ρ_a	Inertia coupling $[kg/m^3]$	0.057	0.23

Table 2 General porous material data.

Symbol	Parameter	Value
η	Dynamic viscosity $[kg/m/s]$	18.4×10^{-6}
P_r	The Prandtl number	0.71
γ_s	Ratio of specific heats	1.4
P_0	Air pressure at reference temperature $[Pa]$	1.01×10^5
ρ_0	Density of fluid in pores $[kg/m^3]$	1.205

To measure the SRI, the specimen is mounted in a wooden frame. The mounting is realised via pins nailed to the frame and clamping the aluminium panel, Figure 2; damping material is used between the aluminium panel and the pins, to avoid contact and rattling noise; the gap between the wooden frame and the aluminium panel is sealed using tape, Figure 2, whereas the gap between the wooden frame and the rubber mat is sealed using mastic, Figure 4. The position of the metal pins is shown in Figure 3. Later, the specimen mounted in the wooden

frame is inserted in a rigid wall for performing the sound reduction index measurement, see next subsection.

Table 3 Porous material parameters.

Symbol	Parameter	Formula
ν	Kinetimatic viscosity	η/ρ_0
ν'	Inverse thermal diffusivity	ν/P_r
q_0	Viscous static permeability	η/σ
q_0'	Thermal static permeability	$\phi\Lambda'^2/8$

Table 4 Bulk modulus of the equivalent fluid [Pa]

Frequency	*Grey*	*Yellow*
80	1.3433e+05 - 0.15113i	96680 - 806.15i
100	1.3433e+05 - 0.13518i	96692 - 1007.2i
125	1.3433e+05 - 0.12091i	96712 - 1258.1i
160	1.3433e+05 - 0.10687i	96748 - 1608.3i
200	1.3433e+05 - 0.095586i	96798 - 2006.7i
250	1.3433e+05 - 0.085495i	96877 - 2501.3i
315	1.3433e+05 - 0.076165i	97005 - 3137i
400	1.3433e+05 - 0.06759i	97213 - 3953.1i
500	1.3433e+05 - 0.060454i	97516 - 4886.3i
630	1.3433e+05 - 0.053857i	97996 - 6046.8i
800	1.3433e+05 - 0.047793i	98751 - 7458.8i
1000	1.3433e+05 - 0.042747i	99791 - 8945.8i
1250	1.3433e+05 - 0.038234i	1.0125e+05 - 10520i
1600	1.3433e+05 - 0.033795i	1.0344e+05 - 12198i
2000	1.3433e+05 - 0.030227i	1.0594e+05 - 13445i
2500	1.3433e+05 - 0.027036i	1.0881e+05 - 14231i
3150	1.3433e+05 - 0.024085i	
4000	1.3433e+05 - 0.021374i	
5000	1.3433e+05 - 0.019117i	

Table 5 Viscous drag [Pa.s/m^2]

Frequency	*Grey*	*Yellow*
80	49817 - 325.2i	17166 - 713.23i
100	49818 - 406.49i	17174 - 891.11i
125	49819 - 508.11i	17187 - 1113i
160	49820 - 650.35i	17210 - 1422.8i
200	49823 - 812.9i	17243 - 1775.1i
250	49827 - 1016.1i	17293 - 2212.4i
315	49833 - 1280.1i	17374 - 2774.7i
400	49843 - 1625.2i	17504 - 3497.3i
500	49858 - 2030.8i	17688 - 4326.1i
630	49882 - 2557.6i	17971 - 5365.2i
800	49922 - 3245.2i	18397 - 6655.1i
1000	49981 - 4051.7i	18956 - 8073.4i
1250	50072 - 5055.4i	19708 - 9707i
1600	50232 - 6450.2i	20802 - 11771i
2000	50459 - 8026.6i	22061 - 13875i
2500	50803 - 9965.2i	23600 - 16212i
3150	51342 - 12424i	
4000	52179 - 15524i	
5000	53314 - 18992i	

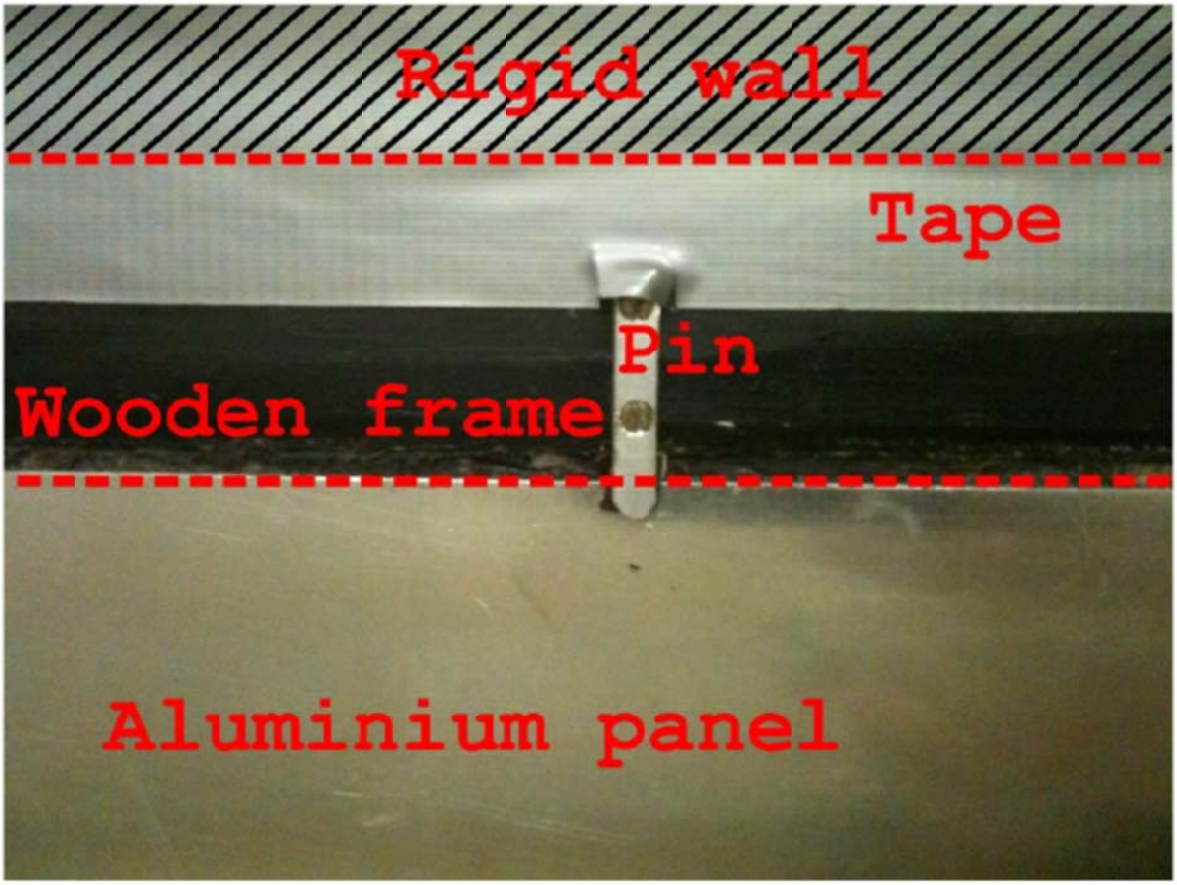

Figure 2 Pins clamping the aluminium panel; the aluminium panel is in the lower half, the wooden frame is in between the two dashed lines and the top half is the rigid wall. The tape seals the gap between the wooden frame and the rigid wall.

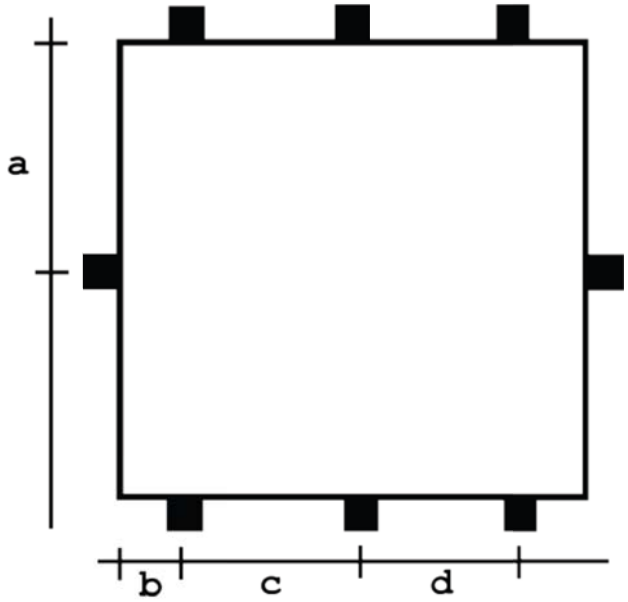

Figure 3 Location of the metal pins on the aluminium panel. Distance **a**: 40.6 cm; Distance **b**: 9.6 cm; Distance **c**: 31.3 cm; Distance **d**: 39 cm.

Table 6 Young's modulus **[**Pa] and shear modulus [Pa] for *Grey*.

Frequency	E_y	G_{xy}
80	1.1794e+05 - 60116i	2.8809e+05 - 1.0547e+05i
100	1.1072e+05 - 52529i	2.7404e+05 - 93813i
125	1.0474e+05 - 45362i	2.6211e+05 - 82315i
160	99467 - 38016i	2.5132e+05 - 70041i
200	95805 - 31988i	2.4364e+05 - 59603i
250	93049 - 26606i	2.3777e+05 - 50021i
315	90987 - 21753i	2.3331e+05 - 41183i
400	89514 - 17503i	2.3009e+05 - 33308i
500	88587 - 14195i	2.2804e+05 - 27103i
630	87947 - 11373i	2.2662e+05 - 21766i
800	87520 - 9013.6i	2.2567e+05 - 17277i
1000	87264 - 7238.5i	2.251e+05 - 13888i
1250	87098 - 5805.3i	2.2473e+05 - 11145i
1600	86982 - 4543.3i	2.2447e+05 - 8725.8i
2000	86916 - 3638.2i	2.2432e+05 - 6989.3i
2500	86873 - 2912.4i	2.2423e+05 - 5595.8i
3150	86846 - 2312.4i	2.2417e+05 - 4443.5i
4000	86827 - 1821.5i	2.2413e+05 - 3500.4i
5000	86817 - 1457.4i	2.241e+05 - 2800.9i

Table 7 Young's modulus [Pa] and shear modulus [Pa] for *Yellow*.

Frequency	E_y	G_{xy}
80	6159.3 - 3190.5i	13523 - 6845.4i
100	5774.3 - 2793.8i	12690 - 6002.5i
125	5453.9 - 2418.6i	11995 - 5202.7i
160	5169.5 - 2032.9i	11377 - 4378.1i
200	4970.1 - 1715.1i	10943 - 3696.9i
250	4818.8 - 1430i	10613 - 3084.7i
315	4704.6 - 1171.7i	10364 - 2528.9i
400	4622.5 - 944.46i	10185 - 2039.2i
500	4570.5 - 766.92i	10071 - 1656.3i
630	4534.4 - 615.02i	9992.1 - 1328.5i
800	4510.3 - 487.73i	9939.3 - 1053.7i
1000	4495.8 - 391.83i	9907.6 - 846.58i
1250	4486.4 - 314.33i	9887 - 679.16i
1600	4479.8 - 246.04i	9872.5 - 531.63i
2000	4476 - 197.05i	9864.3 - 425.78i
2500	4473.6 - 157.75i	9859.1 - 340.86i

Table 8 Rubber mat's data. † indicates a guess.

-	*Grey*	*Yellow*
Poisson's ratio [-] †	0.5	0.5
Density $[kg/m^3]$	1821.5	1470
Thickness $[m]$	3.3×10^{-3}	2.0×10^{-3}

Table 9 Rubber mats shear modulus [Pa].

Frequency	*Grey*	*Yellow*
80	5.7697e+06 - 8.2502e+05i	2.0101e+06 - 5.0863e+05i
100	5.8853e+06 - 8.6461e+05i	2.0778e+06 - 5.4873e+05i
125	6.0065e+06 - 9.0609e+05i	2.151e+06 - 5.9198e+05i
160	6.1473e+06 - 9.543e+05i	2.2386e+06 - 6.4381e+05i
200	6.281e+06 - 1.0001e+06i	2.3244e+06 - 6.9455e+05i
250	6.4211e+06 - 1.0481e+06i	2.417e+06 - 7.493e+05i
315	6.5734e+06 - 1.1002e+06i	2.5206e+06 - 8.1055e+05i
400	6.7387e+06 - 1.1568e+06i	2.6365e+06 - 8.7914e+05i
500	6.9008e+06 - 1.2123e+06i	2.7537e+06 - 9.4843e+05i
630	7.0769e+06 - 1.2726e+06i	2.8848e+06 - 1.026e+06i
800	7.2681e+06 - 1.338e+06i	3.0316e+06 - 1.1128e+06i
1000	7.4556e+06 - 1.4022e+06i	3.1799e+06 - 1.2005e+06i
1250	7.6521e+06 - 1.4695e+06i	3.3399e+06 - 1.2951e+06i
1600	7.8804e+06 - 1.5477e+06i	3.5316e+06 - 1.4085e+06i
2000	8.0973e+06 - 1.6219e+06i	3.7194e+06 - 1.5195e+06i
2500	8.3246e+06 - 1.6998e+06i	3.9219e+06 - 1.6393e+06i
3150	8.5715e+06 - 1.7843e+06i	
4000	8.8396e+06 - 1.8761e+06i	
5000	9.1025e+06 - 1.9661e+06i	

Figure 4 White mastic sealing the gap between the rubber mat and the wooden frame.

2.1 SRI measurement

The SRI measurement follows the ISO 15186 - 1:2000, Measurement of sound insulation in buildings and of building elements using sound intensity.

Figure 5 shows the set-up of the measurement. The specimen presented in the previous section is first mounted in the wooden frame and then installed in a rigid wall in between the anechoic room and the reverberation room in the MWL, with the aluminium panel facing the former room and the rubber mat the latter, see Figures 5-7. Tape and mineral wool are employed to seal the gap between the wooden frame and the rigid wall and, thus, to avoid unwanted sound leakage. In the anechoic room an intensity probe measures the sound

intensity level (probe model 2260, in conjunction with Larson Davis Real time analyzer 2900); in the reverberation room a microphone on a rotating stand measures the space-averaged sound pressure level (half-inch microphone, together with a PC running SpectraPLUS); the sound pressure is generated by four loudspeakers driven by white noise generated by a B&K Noise generator type 1405 and amplified by a NAD 310. Both measurements are done in third-octave bands. The cut-off frequency of the anechoic room is 80 Hz and its dimensions are 7.00 m x 5.95 m x 5.80 m; the dimensions of the reverberation room are 6.21 m x 7.86 m x 5.05 m.

The employed intensity probe allows measurements up to 5 kHz. The quality factor of the intensity measurement, i.e. the difference between intensity and pressure levels, is acceptable till 5 kHz for *Grey* and 2.5 kHz for *Yellow*; at higher frequencies the assumption of no reflections in the anechoic room may be violated due to the measurement procedure, e.g. by the person measuring intensity (see also Figure 7). The field in the reverberant room is diffuse between 50 Hz and 10 kHz. The SRI measurements are considered valid between 80 Hz and 2.5 kHz for *Yellow* and 80 Hz and 5 kHz for *Grey*. In this frequency ranges, the repeatability of the measurement is reliable: the same result is obtained if the plate is mounted, dismounted and remounted, and also if the intensity scanning is done in different fashions.

The space-averaged sound pressure level in third-octave bands L_P is acquired via SpectraPLUS installed on a PC; the space-averaged sound intensity level in third-octave bands L_{In} is measured via a Larson-Davis real-time analyser. The sound reduction index SRI is calculated in MATLAB® using the formula provided in the standard:

$$\mathrm{SRI} = L_P - 6 - L_{In} \,. \tag{4}$$

The SRIs of *Yellow* and *Grey* are reported in Table 10; Figures 9 and Figure 10 show the plot of the SRIs: the *Yellow* and *Grey* SRI show similar trends. Curiously, at lower frequency *Grey* shows a clear plateau, whereas *Yellow* oscillates more.

It is interesting to notice that the measured SRIs have similar trends to those of typical building-construction double-walls presented in Reference [3]. Based upon this fact, a statistical energy analysis for these multilayered structures is introduced in the next section.

3 Statistical energy analysis employing an equivalent fluid

The first step in any SEA is the identification of the elements. An option may be to identify an element with a physical substructure. This choice, however, is not optimal if within a substructure, or due to the interaction of two or more substructures, various wave-types exist. Therefore, a preferred choice is to assign SEA elements to the wave-types. Once the elements are identified, the equations expressing the energy balance between the elements are evaluated. The unknowns in these equations are the modal energy of each SEA element, where modal energy is the total energy divided by the (asymptotic) modal density, or number of modes per unit frequency. The losses in SEA may be of two different kinds: those accounting for internal losses, quantified by the modal overlap factor, and those accounting for coupling losses, quantified by the conductivity.

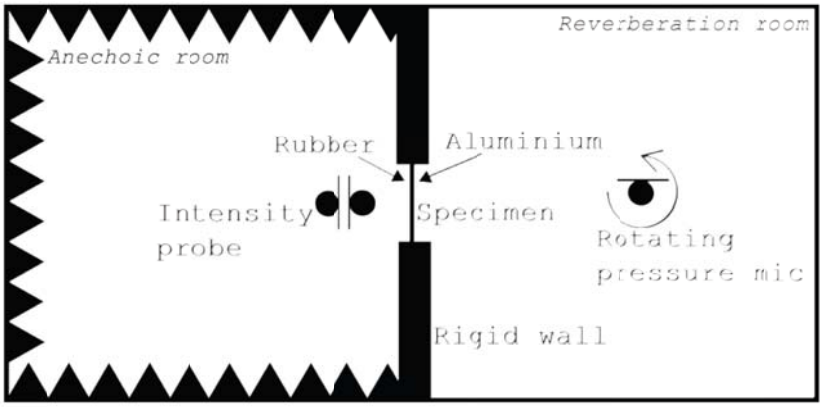

Figure 5 Schematic sketch of the measurement set-up.

Figure 6 View of the multilayered structure from the reverberation room, where a rotating micrhophone measures the spatial-averaged rms pressure.

Reference [3] presents the derivation of the SEA elements for a double-wall. Herein, the same approach is used to derive the SEA for the multilayered structures, which may as well be considered as double walls: the aluminium panel and the rubber mat are the two walls and the porous material is the medium in between them. In particular, the porous material of the composite is herein modelled by an equivalent fluid, defined in Subsection 3.1. The employed SEA elements are:

1. an element describing the acoustic waves in the reverberation room;
2. an element describing the bending waves in the aluminium plate;

3. an element describing the family of plane waves due to the coupling between the equivalent fluid and the walls. This family of waves cuts-on at the double-wall resonance frequency (e.g., around 300 Hz for Grey);
4. an element describing the families of oblique cavity waves due to the coupling between the equivalent fluid and the walls. These families of waves cut-on at frequencies whose half-wavelength is an integer fraction of the distance between the walls (e.g., the first cut-on around 7.5 kHz and the second around 15 kHz for Grey);
5. an element describing the bending waves in the rubber mat;
6. an element describing the acoustic waves in the anechoic room;

Table 10 Sound reduction index measurement in third-octave bands.

f [Hz]	*Yellow* [dB]	*Grey* [dB]
80	4.3	16.3
100	14.4	20.6
125	14.8	21.7
160	14.2	20.8
200	15.4	22.1
250	12.9	21.5
315	12.8	22.4
400	19.7	22.2
500	28.5	19.3
630	34.1	23.1
800	38.3	32.8
1000	42.9	38.8
1250	40.7	42.2
1600	40.4	43.0
2000	38.7	44.9
2500	38.2	47.1
3150	-	51.6
4000	-	53.3
5000	-	54.3

In the SEA derived in Reference [3], Elements 3 and 4 are an original contribution compared to standard SEAs for double-wall structures and their employment actually increases the performance of the SEA. The key idea in that work is to replace the old SEA element describing the double-wall cavity with elements referring to specific wave-types, like Elements 3 and 4. Below the double-wall resonance frequency it is assumed that the walls move in phase, and that the transmission loss is approximately given by the field-incidence mass law:

$$R_{ML} = 10\log\left(1+\left(\frac{m_{tot}\omega}{2\rho c}\right)\right)-5\,, \tag{5}$$

where m_{tot} is the total mass of the double-wall.

The scheme of the proposed SEA is shown in Figure 8, where the channels of energy between the various elements are also visualised. As explained in Section 4, a channel directly connecting the aluminium panel and the rubber mat may be employed to account for possible direct energy flows between them (see **G** in Figure 8). Reference [3] presents expressions for all conductivities and modal densities of the elements in Figure 8.

Figure 7 View of the multilayered structure from the anechoic room, where an intensity probe measures the time-averaged intensity.

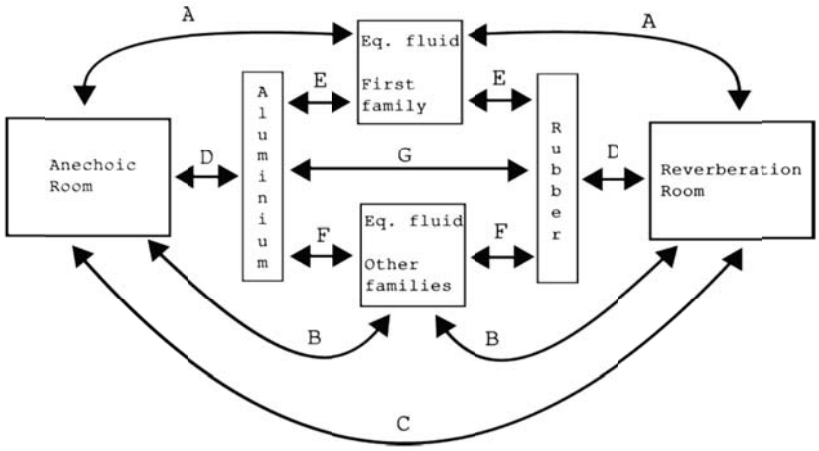

Figure 8 Proposed SEA for a multilayered structure. **A**, mass impeded equivalent fluid-wall element ↔room channel; **B**, oblique equivalent fluid - wall element ↔room channel; **C**, rooms ↔room channel (mass law, non-resonant); **D**, room ↔wall channel; **E**, mass impeded plane equivalent fluid - wall element ↔wall channel; **F**, oblique equivalent fluid-wall element ↔channel; **G**, wall ↔wall channel (flanking transmission).

3.1 The equivalent fluid

In the statistical energy analysis of these structures an equivalent fluid substitutes for the porous material in the composite. This fluid has bulk modulus and density equivalent to those of the porous material, which are taken from Reference [4]. A similar approach is used by Morse and Ingard to study the propagation of sound wave in porous media with rigid frames [5]. The bulk modulus of the equivalent fluid reads

$$R_e = \phi\gamma_s P_0 \left[\gamma_s - \frac{\gamma_s - 1}{1 + \frac{\nu'\phi}{i\omega q_0'} G'} \right], \tag{6}$$

where

$$G' = 1 + \left(\frac{2q_0'}{\phi\Lambda'} \right)^2 \frac{i\omega}{\nu'}, \tag{7}$$

and the other quantities are detailed in Tables 1-3. The density of the equivalent fluid reads:

$$\rho_e = \phi\rho_0 + \rho_a - \frac{ib}{\omega}, \tag{8}$$

where ρ_0 is the density of the fluid in the pores, ρ_a is the additional mass due to the inertia coupling between the pore-fluid and the frame and *b* is the viscous drag; the expressions of the two last quantities are given by:

$$\rho_a = \phi\rho_0 \left(\alpha_\infty - 1 \right), \tag{9}$$

and

$$b = \sigma\phi^2 G, \tag{10}$$

where α_∞ is the tortuosity, σ is the static flow resistance and

$$G = 1 + \left(\frac{2\alpha_\infty q_0}{\phi\Lambda} \right)^2 \frac{i\omega}{\nu}. \tag{11}$$

Table 3 details the remaining quantities; see Reference [4] for further details on these quantities. The velocity of the equivalent fluid follows:

$$c_e = \sqrt{\frac{R_e}{\rho_e}}. \tag{12}$$

The sound in the equivalent fluid satisfies Helmholtz equations and is between the two walls, which are parallel to the *x*-*y* plane and are separated by a distance *z*=*d*. For harmonic motion $e^{-i\omega t}$, the equations of motion of the fluid and of the walls are

$$\begin{aligned} \Delta\tilde{p} + k_e^2 \tilde{p} = 0; \qquad & k_e = \frac{\omega}{c_e}; \\ B_w \nabla\tilde{u}_w - m_w\omega^2\tilde{u} = \nu_w\tilde{p}; \qquad & \nu_1 = -1; \nu_2 = 2, \end{aligned} \tag{13}$$

Where $\tilde{p}$ is the time rms sound pressure in the equivalent fluid and $\tilde{u}_w$ is the time rms displacement in the transverse direction of wall *w* (i.e., the aluminium panel and the rubber mat). The wall velocities equal the equivalent-fluid velocity at their interfaces and it follows that

$$-i\omega\tilde{u}_w = \frac{1}{i\rho_e\omega} \frac{\partial\tilde{p}\left(x, y, z = z_w, \omega\right)}{\partial z}; \quad z_1 = 0; \quad z_2 = d. \tag{14}$$

The internal losses of the equivalent fluid may be either thermal losses, related to the bulk modulus, or viscous losses, related to the viscous drag. Thus, the damping loss factor for the equivalent fluid-wall elements is calculated as:

$$\eta_r = \frac{\Im(R_e)}{\Re(R_e)} + \frac{\Im(v)}{\Re(v)}, \tag{15}$$

where $\Im$ and $\Re$ are the imaginary and real parts of a complex number and *v* reads:

$$v = \frac{b}{\omega \rho_e}. \tag{16}$$

4 Results

The comparison between the SEA presented in the previous section and the measurement presented in Section 2 is shown in Figures 9-12 for *Grey* and *Yellow*. The performance of SEA is overall good.

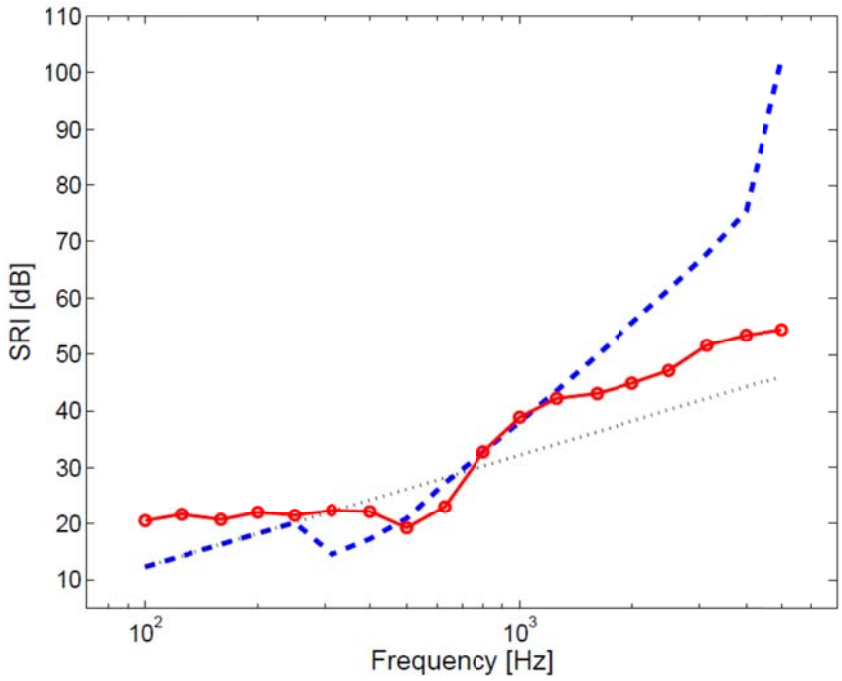

Figure 9 SRI for the multilayered structure comprising the *Grey* material: measurement (red curve with circles), SEA (blue dashed curve) and mass-law prediction (black dotted curve). The SEA model employs no direct coupling between the walls.

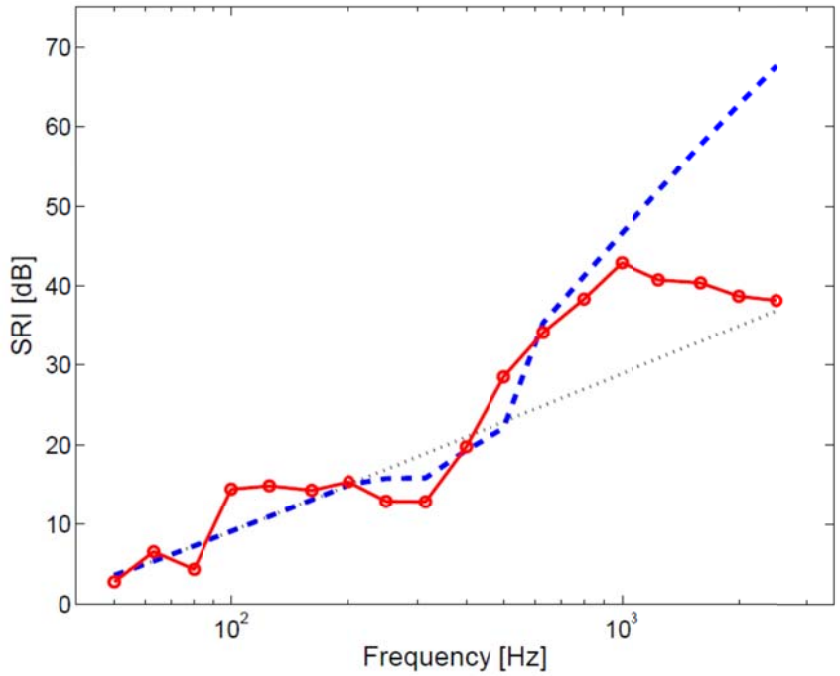

Figure 10 SRI for the multilayered structure comprising the *Yellow* material: measurement (red curve with circles), SEA (blue dashed curve) and mass-law prediction (black dotted curve). The SEA model employs no direct coupling between the walls.

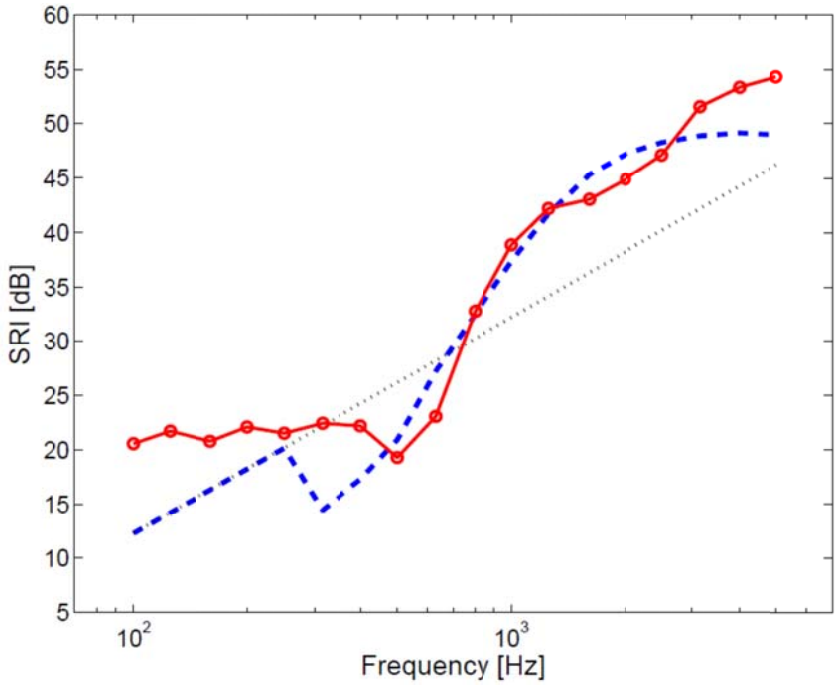

Figure 11 SRI for the multilayered structure comprising the *Grey* material: measurement (red curve with circles), SEA (blue dashed curve) and mass-law prediction (black dotted curve). The SEA model employs a coupling loss factor of 2.5×10^{-3} between the walls.

At low frequencies around the double-wall resonance the prediction is acceptable for *Yellow*, while somewhat erratic for *Grey*. The reason might be a very low mode count in these frequency bands. At middle frequencies, the SEA provides a very good prediction, since both the level and the slope are correct; note that the mass-law no longer predicts the

measurement. At higher frequencies SEA underestimates the response, as Figures 9-10 show. The SEA does not include any flanking transmission between the two walls, as they are not directly connected. However, there might be unwanted flanking transmission in the measurement, leading to a direct energy flow between the walls. The employment of an equivalent fluid for modelling the porous material, besides, discards the motion of its frame, which can also transfer energy between the two walls. In order to account for these energy flows, an ad-hoc channel between the walls may be added, see **G** in Figure 8. Figures 11-12 show the improved performance of SEA when the two walls are connected via a coupling loss factor of the order of 10^{-3} for *Yellow* and 10^{-4} for *Grey*, which are very small very small compared to the damping loss factor that are of the order of 10^{-1}. These values are obtained with a curve-fitting between the measurements and the SEA predictions of Figures 9-10.

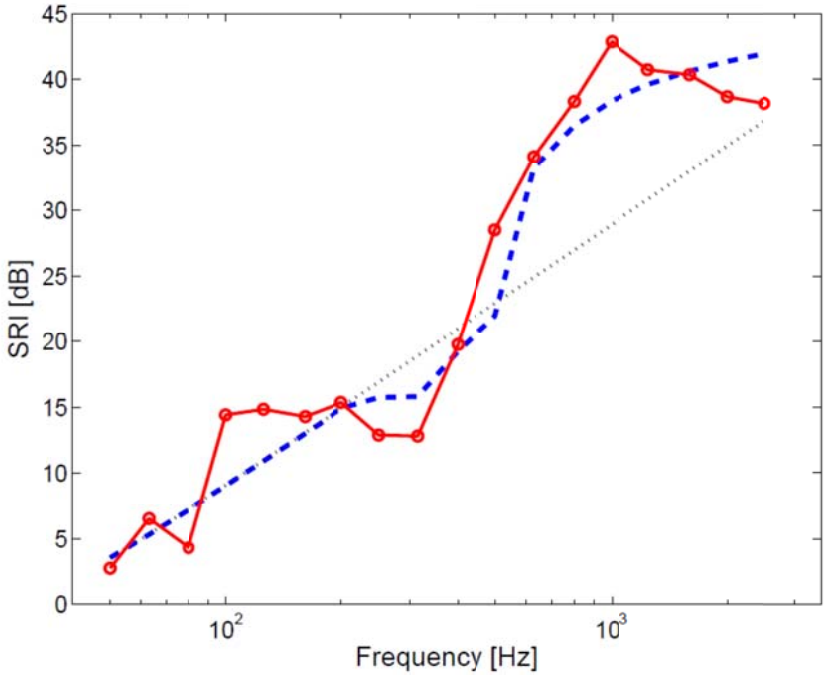

Figure 12 SRI for the multilayered structure comprising the *Yellow* material: measurement (red curve with circles), SEA (blue dashed curve) and mass-law prediction (black dotted curve). The SEA model employs a coupling loss factor of 1.3 x 10^{-4} between the walls.

5 Acknowledgments

The following acknowledgments are kindly given: EC Mid-Mod for economical support; Danilo Prelevic, Leiping Feng, Ulf Carlsson and Kent Lindgren for helping with the measurements.

6 References

[1] P. Göransson Personal communication.

[2] M. Barbagallo, S. Finnveden TRITA-AVE - A cavity-wall element for the statistical energy analysis of double walls.

[3] J. F. Allard, N. Atalla Propagation of Sound in Porous Media, 2nd edition, Wiley, Chap. 6, pp. 111-135, 2009.

[4] P. M. Morse, K. U. Ingard Theoretical Acoustics Princeton University Press, Sec. 6.4, pp. 251, 1986.